JACS
JOURNAL OF THE AMERICAN CHEMICAL SOCIETY

COMMUNICATION

pubs.acs.org/JACS

Solid-State Spin Crossover of Ni(II) in a Bioinspired N_3S_2 Ligand Field

Huaibo Ma,[†] Jeffrey L. Petersen,[‡] Victor G. Young, Jr.,[§] Gordon T. Yee,[∥] and Michael P. Jensen*[,†]

[†]Department of Chemistry and Biochemistry, Ohio University, Athens, Ohio 45701, United States

[‡]C. Eugene Bennett Department of Chemistry, West Virginia University, Morgantown, West Virginia 26506, United States

[§]X-ray Crystallographic Facility, Department of Chemistry, University of Minnesota, Minneapolis, Minnesota 55455, United States

[∥]Department of Chemistry, Virginia Polytechnic Institute and State University, Blacksburg, Virginia 24061, United States

Supporting Information

ABSTRACT: The complex $Tp^{Ph,Me}NiS_2CNMe_2$ [$Tp^{Ph,Me}$ = hydrotris(3-phenyl-5-methyl-1-pyrazolyl)borate] features a bioinspired N_3S_2 ligand set supporting a five-coordinate, trigonally distorted square-pyramidal geometry in the solid state. Spin crossover of Ni(II) was demonstrated by temperature-dependent X-ray crystallography and magnetic susceptibility measurements. The crystal lattice contains two independent molecules (i.e., Ni1 and Ni2). At 293 K, the observed bond lengths and susceptibility are consistent with high-spin (S = 1) Ni(II), and both molecules exhibit relatively short axial Ni−N bonds and long Ni−N and Ni−S equatorial bonds. At 123 K, the Ni1 complex remains high-spin, but the Ni2 molecule substantially crosses to a structurally distinct diamagnetic (S = 0) state with significant elongation of the axial Ni−N bond and offsetting contraction of the equatorial bonds. The temperature-dependent susceptibility data were fit to a spin equilibrium at Ni2 [ΔH° = 1.13(2) kcal/mol and ΔS° = +7.3(1) cal mol^{-1} K^{-1}] consistent with weak coupling to lattice effects. Cooling below 100 K results in crossover of the Ni1 complex.

Spin crossover is a means to obtain bistable molecular switches for nanoscale devices.[1,2] Cooperative intermolecular behavior in the solid state can lead to abrupt spin transitions with thermal hysteresis, enabling bistability and optical switching.[3] This phenomenon is usually defined to include octahedral $3d^4$−$3d^7$ metal ions, and a majority of examples involve crossing of d^6 Fe(II) from a low-spin state to a high-spin state (i.e., $^1A_{1g} \rightarrow {}^5T_{2g}$) in which isotropic ligand breathing is coupled to $t_{2g} \rightarrow e_g$ electron unpairing.[4]

In contrast, "anomalous magnetism" of d^8 Ni(II) complexes typically involves ligand addition or a conformational change.[4,5] For example, $(Ph_2BnP)_2NiBr_2$ crystallizes as a mixture of square-planar diamagnetic (S = 0) and tetrahedral paramagnetic (S = 1) "allogons".[6] Nonallogonic spin crossover of Ni(II) is also possible through axial modulation of a tetragonal ligand field; $^3B_{1(g)} \leftrightarrow {}^1A_{1(g)}$ spin crossover can be attained for a d^8 metal ion under axial C_{4v} (D_{4h}) distortion.[5,7−15] Dynamic ligand field rearrangements are difficult to achieve in the solid state.[13] Nevertheless, the solid-state anomalous magnetism of a few penta- and hexacoordinate Ni(II) complexes has long been attributed to spin crossover,[5,14−21] but the relevant spin isomers have not been structurally characterized.[11] In the present work, we obtained magnetic and structural evidence for solid-state spin crossover of pentacoordinate Ni(II) in a bioinspired N_3S_2 ligand field.

The inspiration for our work was the nickel-dependent superoxide dismutase, which recently was structurally characterized as a mixture of Ni(III) in a square-pyramidal N_3S_2 ligand field (including the N-terminal amine, the adjacent backbone amide, Cys-2 and -6 thiolates, and an axial His-1 imidazole) and Ni(II) in a square-planar N_2S_2 ligand field (with a detached axial imidazole).[22,23] Retention of the latter ligand in a reduced catalytic intermediate would give square-pyramidal spin isomers that are either elongated and diamagnetic (S = 0) or compressed and paramagnetic (S = 1), depending on the strength of the interaction.[24,25]

We previously reported Ni(II) complexes of facially tridentate hydrotris(pyrazolyl)borate chelates [hydrotris(3-R-5-methyl-1-pyrazolyl)borate: R = Me ($Tp^{Me,Me}$), Ph ($Tp^{Ph,Me}$)][26] with zwitterionic dithiocarbamate ($R'_2NCS_2^-$: R′ = Et, Ph) coligands as models for the biologically unique NiSOD active site.[27,28] These synthetic complexes exhibit a κ^3-/κ^2-$Tp^{R,Me}$ scorpionate equilibrium in solution between a green paramagnetic N_3S_2 isomer and a red diamagnetic N_2S_2 isomer with a detached axial pyrazolyl donor. An analogous spin equilibrium driven by ene−allyl cyclopentadienyl ring slippage was observed in solution for $C_5Me_5Ni(acac)$.[29] Sterically unhindered $Tp^{Me,Me}NiS_2CNEt_2$ crystallized as a green square pyramid in the solid state[27] with a κ^3-Tp ligand and slight trigonal distortion (τ = 0.31),[30] while the bulkier $Tp^{Ph,Me}NiS_2CNR_2$ (R = Et, Ph) complexes both crystallized as red square planes (τ = 0.01) with κ^2-Tp ligands.[28] In the present work, we prepared $Tp^{Ph,Me}NiS_2CNMe_2$, which has intermediate bulkiness, and isolated a green crystalline solid that exhibits spin crossover (for synthesis and characterization, see the Supporting Information).

Two structure determinations were performed on separate crystals of $Tp^{Ph,Me}NiS_2CNMe_2$ at 293 and 123 K. The crystal data are summarized in Table 1, and coordinate bond lengths are given in Table 2. Essentially identical triclinic $P\bar{1}$ lattices were observed at both temperatures (Table 1 and Figure 1), with 1.0−1.5% contractions in the unit cell axes and a 3.1% reduction in unit cell volume at the lower temperature. The lattices contain two independent molecules (i.e., Ni1 and Ni2; Figure 2), both of

Received: December 3, 2010
Published: March 28, 2011

which are pentacoordinate and approximately square-pyramidal (τ = 0.28 and 0.32 for Ni1 and Ni2, respectively, at 293 K).

Consistent with the green color of the crystals, the overall structure of the Ni1 site compares well with the high-spin $Tp^{Me,Me}NiS_2CNEt_2$ analogue (Table 2).[27] The coordinate bond lengths are consistent with single-electron occupation of both the axial and equatorial dσ^* orbitals in a high-spin (S = 1) d^8 electron configuration. The Ni1 complex displays a relatively short apical Ni1−N1 bond length of 2.048(1) Å and an axial H−B1−N2−N1 torsion angle of 179.6(2)° at 293 K, while the equatorial Ni−N and Ni−S bond lengths are significantly longer than those in the red κ^2-$Tp^{Ph,Me}NiS_2CNEt_2$ complex.[28] Trigonal distortion is evident, with an axis along the N3−Ni1−S1 bond vector of 172.10(4)°. The Ni1 structure at 123 K is essentially identical.

The Ni2 site displays a longer apical Ni−N bond length of 2.149(1) Å at 293 K, with a decreased H−B2−N9−N11 torsion angle of 167.2(2)°. Shorter equatorial bond lengths are also apparent (Table 2). While the Ni1 site is invariant between 293 and 123 K (Table 2 and Figure 2), Ni2 at 123 K exhibits a further increase of the axial bond length to 2.401(2) Å with decreases in the H−B−N−N torsion angle to 163.5(2)° and the τ value to 0.22. Contractions of the equatorial bonds are also observed.

Table 1. Summary of the X-ray Structure Determinations

T (K)	293(2)	123(2)
empirical formula	$C_{33}H_{34}BN_7NiS_2$	$C_{33}H_{34}BN_7NiS_2$
formula weight	662.31	662.31
crystal system	triclinic	triclinic
space group	$P\bar{1}$	$P\bar{1}$
a (Å)	12.1442(8)	12.004(1)
b (Å)	12.6611(9)	12.536(1)
c (Å)	25.058(2)	24.678(2)
α (deg)	90.556(1)	91.034(1)
β (deg)	102.357(1)	101.353(1)
γ (deg)	116.994(1)	116.788(1)
V (Å^3)	3328.3(4)	3225.9(5)
Z	4	4
d_{calcd} (g/cm^3)	1.322	1.364
R_1 [$I > 2\sigma(I)$]	0.0500	0.0373
wR_2 [$I > 2\sigma(I)$]	0.1373	0.0849
R_1 (all data)	0.0632	0.0525
wR_2 (all data)	0.1496	0.0934
goodness of fit	1.029	1.040

This is consistent with spin crossover, suggesting that the Ni2 site represents a temperature-dependent superposition of spin isomers. Elongated square-pyramidal geometries were observed for diamagnetic $Tp^{Me,Me}Ni(CN)_2$,[31] $TpNi(PMe_3)Ph$,[32] and $TpNi(\eta^3\text{-}C_3H_5)$.[33,34]

The high-spin fractions at Ni2 can be estimated from the observed equatorial bond lengths, taking the averaged Ni1 values as the high-spin limit and those for square-planar κ^2-$Tp^{Ph,Me}NiS_2CNEt_2$ as the low-spin limit (Table 2). Linear interpolation between these values gives high-spin fractions of 38 ± 2% at 123 K and 87 ± 5% at 293 K. Back-extrapolation of a limiting Ni−N axial bond length for the low-spin square pyramid gives a value of 2.62 Å from the 123 K data, compared with the average value of 2.04 Å for high-spin Ni1. Corresponding square-pyramidal spin isomers of reduced NiSOD have not been observed experimentally, but axial Ni−N(His1) bond lengths of 2.612 and 1.958 Å were calculated for the low- and high-spin states, respectively, using density functional theory.[25]

To confirm the spin crossover, solid-state magnetic susceptibility measurements were performed for $Tp^{Ph,Me}NiS_2CNMe_2$ from 5 to 300 K (Figure 3). The susceptibility observed at 300 K, χT = 1.40 emu K/mol (μ = 3.35μ_B), is consistent with an S = 1 ground state and second-order spin−orbit coupling; for comparison, previous measurements for $Tp^{Me,Me}NiS_2COMe$ fit the Curie law, with χT = 1.42 emu K/mol (μ = 3.37μ_B) and Θ = −6.1 K.[27] However, the susceptibilities in the present work do not conform to the Curie law. Consistent with this observation and the structural data, the susceptibility data were fit to Maxwell−Boltzmann statistics over the 100−300 K range,

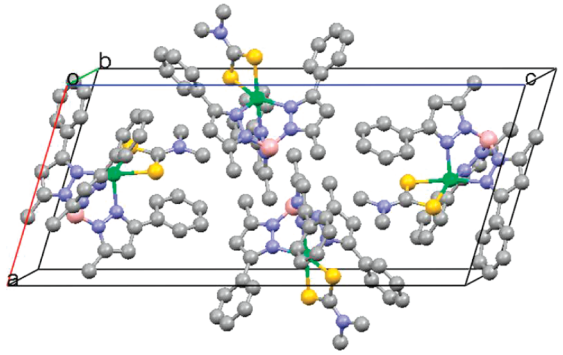

Figure 1. Unit cell of $Tp^{Ph,Me}NiS_2CNMe_2$ at 293 K. The Ni2 sites are disposed to the outside left and right, with the Ni1 sites near the center. Hydrogen atoms have been omitted for clarity.

Table 2. Summary of Bond Lengths and Ligand Field Geometries

	$Tp^{Me,Me}NiS_2CNEt_2$	$Tp^{Ph,Me}NiS_2CNMe_2$ [Ni1]	$Tp^{Ph,Me}NiS_2CNMe_2$ [Ni1]	$Tp^{Ph,Me}NiS_2CNMe_2$ [Ni2]	$Tp^{Ph,Me}NiS_2CNMe_2$ [Ni2]	$Tp^{Ph,Me}NiS_2CNEt_2$
T (K)	293	293	123	293	123	293
Ni−$N_{ax,eq}$ (Å)[a]	2.027(1) [N1]	2.048(1) [N1]	2.038(2) [N1]	2.149(1) [N8]	2.401(2) [N8]	2.805(1) [N6]
Ni−$N_{eq,ax}$ (Å)[a]	2.065(1) [N3]	2.111(1) [N3]	2.111(2) [N3]	2.083(1) [N12]	2.003(2) [N12]	1.934(1) [N3]
Ni−$N_{eq,eq}$ (Å)[a]	2.063(1) [N5]	2.058(1) [N5]	2.048(2) [N5]	2.046(1) [N10]	1.972(2) [N10]	1.929(1) [N1]
Ni−$S_{eq,eq}$ (Å)[a]	2.3747(8) [S1]	2.3435(5) [S2]	2.3420(6) [S2]	2.3234(6) [S4]	2.2567(6) [S4]	2.1990(5) [S1]
Ni−$S_{eq,ax}$ (Å)[a]	2.4099(7) [S2]	2.3929(5) [S1]	2.4006(6) [S1]	2.3614(5) [S3]	2.2721(7) [S3]	2.1929(5) [S2]
H−B−N−N_{ax} (deg)	176.0(2)	179.6(2)	179.9(2)	167.2(2)	163.5(2)	133.2(2)
τ[b]	0.31	0.28	0.29	0.32	0.22	0.01
reference	27	this work	this work	this work	this work	28

[a] Ligand positions refer to (major, minor) square pyramidal, trigonal geometries. [b] Defined as in ref 30.

dx.doi.org/10.1021/ja110890v | J. Am. Chem. Soc. 2011, 133, 5644–5647

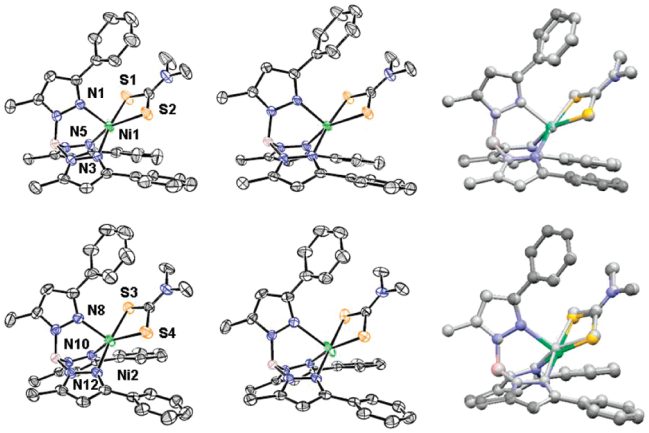

Figure 2. ORTEP plots of $Tp^{Ph,Me}NiS_2CNMe_2$ at 293 K (left, 30% ellipsoids) and 123 K (center, 50% ellipsoids) along with overlays of the Ni1 and Ni2 structures (right: 123 K, color; 293 K, graytone) based on least-squares alignments of B1/N4/N6 (top) and B2/N11/N13 (bottom). Hydrogen atoms have been omitted for clarity.

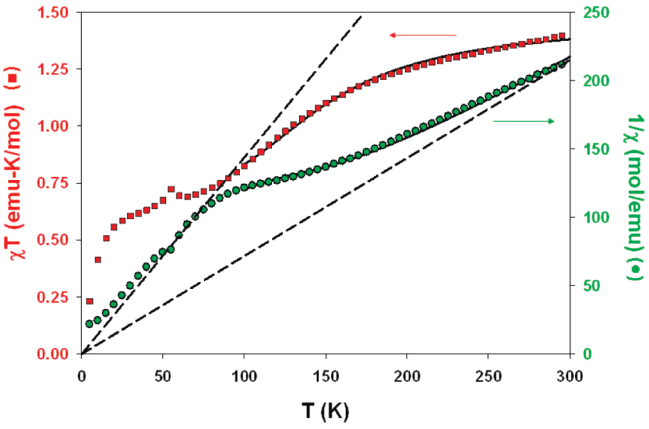

Figure 3. Solid-state temperature-dependent magnetic susceptibility data (χT, left axis; $1/\chi$, right axis) for $Tp^{Ph,Me}NiS_2CNMe_2$. Dashed lines are maximal Curie law slopes for the inverse susceptibility (i.e., $T = C/\chi$; ●, right axis) at high-spin Ni(II) mole fractions of 50 and 100%. Solid curves were calculated from the fit to a spin equilibrium at Ni2 (see the text). The discontinuity near 54 K is assigned to adventitious O_2.

assuming thermal equilibrium of half of the Ni(II) sites (i.e., Ni2) between the $S = 0$, 1 states (Figure 3; for details of the fit, see the Supporting Information). The following thermodynamic parameters were obtained: $\Delta H^\circ = 1.13(2)$ kcal/mol, $\Delta S^\circ = +7.3(1)$ cal mol^{-1} K^{-1}; $T_{1/2} = 155(5)$ K; $\Delta G^\circ_{293K} = -360$ cm^{-1}; $\mu_{HS/HS} = 3.45\mu_B$. Some correlation of residuals was evident, suggesting weak coupling of the crossover to lattice effects. Combined with ligand field rearrangement, this may lead to departure of the crossover entropy from the inherent spin-only value (i.e., $R \ln 3 = +2.2$ cal mol^{-1} K^{-1}).[14] The fit gave estimates of 28(3) and 85(1)% for the high-spin mole fractions of Ni2 at 123 and 293 K, respectively; these are comparable to the values deduced from the X-ray structures at these temperatures (see above).

Because of the effects of zero-field splitting and antiferromagnetic coupling, the data obtained below 100 K were not fit. However, these data are consistent with subsequent crossover of Ni1. Two-step spin crossovers have been documented for a handful of monomeric octahedral complexes and typically reflect the presence of independent complexes in a lattice, which may arise from a phase transition.[35] The crystal structures herein suggest a similar origin for sequential crossover of Ni2 followed by Ni1. The equatorial ligand plane of Ni2 is oriented with the long c axis, while that of Ni1 is nearly orthogonal (Figure 1); thus, the relatively large contraction along c is coincident with equatorial bond contraction at Ni2. These effects may be mediated by a van der Waals contact between a dithiocarbamate substituent on Ni2 and an equatorial pyrazole on Ni1, and also by π-stacking between one equatorial pyrazole ring (i.e., N10) on separate Ni2 complexes, with rigorously parallel interplanar separations of 3.685 Å at 293 K and 3.652 Å at 123 K. Offsetting axial elongation is accomplished by displacement of the nickel atom, rather than the apical pyrazole donor, within the rigid pocket circumscribed by the 3-Ph substituents; the thermal ellipsoid of Ni2 exhibits high eccentricity at 123 K, with the major axis nearly aligned with the axial Ni2−N8 bond vector (Figure 2).

In summary, we have obtained structural and magnetic evidence for an unusual solid-state spin equilibrium in a biomimetic Ni(II) complex. Crossover to low-spin Ni(II) with decreasing temperature results in axial bond elongation and equatorial bond contractions, consistent with electron pairing into the lower axial orbital absent e_g orbital degeneracy. The e_g (i.e., $d\sigma^*$) orbital splitting must be tuned to offset the electron pairing energy and support both spin states with proximal zero-point energies.[3,5] The spin state of pentacoordinate Ni(II) is correlated to ligand donor properties;[9] the N_3S_2 ligand field herein must be nearly optimal for crossover, but whether this is true for the particular donor set of NiSOD remains unknown. $Tp^{Me,Me}NiS_2COMe$ is rigidly paramagnetic (see above),[27] so the heteroatom in the zwitterionic dithioacid coligand and steric contact with the opposing Tp ligand substituents also must be important factors. Finally, the crossover behavior seems correlated with crystal packing. We are endeavoring to exploit all of these unique properties to design new Ni(II) complexes with abrupt spin transitions, which require enhanced coupling of the lattice and ligand field vibrations.[1−4]

■ ASSOCIATED CONTENT

Supporting Information. Details of syntheses, characterization, and susceptibility data and fits; crystallographic data for $Tp^{Ph,Me}NiS_2CNMe_2$ at 293 and 123 K (CIF). This material is available free of charge via the Internet at http://pubs.acs.org.

■ AUTHOR INFORMATION

Corresponding Author
jensenm@ohio.edu

■ ACKNOWLEDGMENT

The authors acknowledge the donors of the American Chemical Society Petroleum Research Fund (49296-DNI3) for support of this research. We thank Prof. Dean Johnston of Otterbein University for assistance with powder X-ray diffraction.

■ REFERENCES

(1) Kahn, O.; Martinez, C. J. *Science* **1998**, *279*, 44–48.
(2) Létard, J.-F.; Guionneau, P.; Goux-Capes, L. *Top. Curr. Chem.* **2004**, *235*, 221–249.

(3) Gütlich, P.; Hauser, A.; Spiering, H. *Angew. Chem., Int. Ed. Engl.* **1994**, *33*, 2024–2054.
(4) Gütlich, P.; Goodwin, H. A. *Top. Curr. Chem.* **2004**, *233*, 1–47.
(5) Barefield, E. K.; Busch, D. H.; Nelson, S. M. *Q. Rev. Chem. Soc.* **1968**, *22*, 457–498.
(6) Kilbourn, B. T.; Powell, H. M. *J. Chem. Soc. A* **1970**, 1688–1693.
(7) Ballhausen, C. J.; Liehr, A. D. *J. Am. Chem. Soc.* **1959**, *81*, 538–542.
(8) Maki, G. *J. Chem. Phys.* **1958**, *29*, 1129–1138.
(9) Sacconi, L. *Coord. Chem. Rev.* **1972**, *8*, 351–367.
(10) Ono, K.; Yoshizawa, M.; Akita, M.; Kato, T.; Tsunobuchi, Y.; Ohkoshi, S.-i.; Fujita, M. *J. Am. Chem. Soc.* **2009**, *131*, 2782–2783.
(11) Ruiz-Martínez, A.; Casanova, D.; Alvarez, S. *Chem.—Eur. J.* **2010**, *16*, 6567–6581.
(12) Szacilowski, K. T.; Xie, P.; Malkhasian, A. Y. S.; Heeg, M. J.; Udugala-Ganehenege, M. Y.; Wenger, L. E.; Endicott, J. F. *Inorg. Chem.* **2005**, *44*, 6019–6033.
(13) Venkataramani, S.; Jana, U.; Dommaschk, M.; Sönnichsen, F. D.; Tuczek, F.; Herges, R. *Science* **2011**, *331*, 445–448.
(14) Melson, G. A.; Busch, D. H. *J. Am. Chem. Soc.* **1964**, *86*, 4830–4833.
(15) Holt, S. L.; Bouchard, R. J.; Carlin, R. L. *J. Am. Chem. Soc.* **1964**, *86*, 519–520.
(16) Goodgame, D. M. L.; Goodgame, M.; Weeks, M. J. *J. Chem. Soc. A* **1967**, 1125–1132.
(17) Bray, K. L.; Drickamer, H. G. *J. Phys. Chem.* **1990**, *94*, 7037–7040.
(18) Nelson, S. M.; Kelly, W. S. J. *Chem. Commun.* **1968**, 436–437.
(19) Kelly, W. S. J.; Ford, G. H.; Nelson, S. M. *J. Chem. Soc. A* **1971**, 388–396.
(20) Dahlhoff, W. V.; Nelson, S. M. *J. Chem. Soc. A* **1971**, 2184–2190.
(21) Yamauchi, J.; Tsuji, H.; Sakai, N.; Kawamura, Y. *Chem. Lett.* **2003**, *32*, 368–369.
(22) Wuerges, J.; Lee, J.-W.; Yim, Y.-I.; Yim, H.-S.; Kang, S.-O.; Djinovic Carugo, K. *Proc. Natl. Acad. Sci. U.S.A.* **2004**, *101*, 8569–8574.
(23) Barondeau, D. P.; Kassmann, C. J.; Bruns, C. K.; Tainer, J. A.; Getzoff, E. D. *Biochemistry* **2004**, *43*, 8038–8047.
(24) Pelmenschikov, V.; Siegbahn, P. E. M. *J. Am. Chem. Soc.* **2006**, *128*, 7466–7475.
(25) Neupane, K. P.; Gearty, K.; Francis, A.; Shearer, J. *J. Am. Chem. Soc.* **2007**, *129*, 14605–14618.
(26) Rheingold, A. L.; Ostrander, R. L.; Haggerty, B. S.; Trofimenko, S. *Inorg. Chem.* **1994**, *33*, 3666–3676.
(27) Ma, H.; Wang, G.; Yee, G. T.; Petersen, J. L.; Jensen, M. P. *Inorg. Chim. Acta* **2009**, *362*, 4563–4569.
(28) Ma, H.; Chattopadhyay, S.; Petersen, J. L.; Jensen, M. P. *Inorg. Chem.* **2008**, *47*, 7966–7968.
(29) Smith, M. E.; Andersen, R. A. *J. Am. Chem. Soc.* **1996**, *118*, 11119–11128.
(30) Addison, A. W.; Rao, T. N.; Reedijk, J.; van Rijn, J.; Verschoor, G. C. *J .Chem. Soc., Dalton Trans.* **1984**, 1349–1356.
(31) Li, D.; Ruschman, C.; Parkin, S.; Clérac, R.; Holmes, S. M. *Chem. Commun.* **2006**, 4036–4038.
(32) Gutiérrez, E.; Hudson, S. A.; Monge, A.; Nicasio, M. C.; Paneque, M.; Ruiz, C. *J. Organomet. Chem.* **1998**, *551*, 215–227.
(33) Lehmkuhl, H.; Näser, J.; Mehler, G.; Kiel, T.; Danowski, F.; Benn, R.; Mynott, R.; Schroth, G.; Gabor, B.; Krüger, C.; Betz, P. *Chem. Ber.* **1991**, *124*, 441–452.
(34) Shirasawa, N.; Nguyet, T. T.; Hikichi, S.; Moro-oka, Y.; Akita, M. *Organometallics* **2001**, *20*, 3582–3598.
(35) Griffin, M.; Shakespeare, S.; Shepherd, H. J.; Harding, C. J.; Létard, J.-F.; Desplanches, C.; Goeta, A. E.; Howard, J. A. K.; Powell, A. K.; Mereacre, V.; Garcia, Y.; Naik, A. D.; Müller-Bunz, H.; Morgan, G. G. *Angew. Chem., Int. Ed.* **2011**, *50*, 896–900.